

Growth of fcc(111) Dy multi-height islands on 6H-SiC(0001) graphene

This article has been downloaded from IOPscience. Please scroll down to see the full text article.

2013 J. Phys.: Condens. Matter 25 225005

(<http://iopscience.iop.org/0953-8984/25/22/225005>)

View [the table of contents for this issue](#), or go to the [journal homepage](#) for more

Download details:

IP Address: 147.155.68.114

The article was downloaded on 30/08/2013 at 21:48

Please note that [terms and conditions apply](#).

Growth of fcc(111) Dy multi-height islands on 6H-SiC(0001) graphene

M T Hershberger^{1,2}, M Hupalo¹, P A Thiel^{1,3,4} and M C Tringides^{1,2}

¹ Ames Laboratory, US Department of Energy, Iowa State University, Ames, IA 50011, USA

² Department of Physics and Astronomy, Iowa State University, Ames, IA 50011, USA

³ Department of Chemistry, Iowa State University, Ames, IA 50011, USA

⁴ Department of Materials Science and Engineering, Iowa State University, Ames, IA 50011, USA

E-mail: tringides@ameslab.gov

Received 27 December 2012, in final form 26 April 2013

Published 15 May 2013

Online at stacks.iop.org/JPhysCM/25/225005

Abstract

Graphene based spintronic devices require an understanding of the growth of magnetic metals. Rare earth metals have large bulk magnetic moments so they are good candidates for such applications, and it is important to identify their growth mode. Dysprosium was deposited on epitaxial graphene, prepared by thermally annealing 6H-SiC(0001). The majority of the grown islands have triangular instead of hexagonal shapes. This is observed both for single layer islands nucleating at the top of incomplete islands and for fully completed multi-height islands. We analyze the island shape distribution and stacking sequence of successively grown islands to deduce that the Dy islands have fcc(111) structure, and that the triangular shapes result from asymmetric barriers to corner crossing.

(Some figures may appear in colour only in the online journal)

1. Introduction

Graphene is a novel material studied extensively over the last 8 years [1–6]. Its unusual electronic structure holds the promise of future applications in many areas, especially for the new generation of ultrafast microelectronics. Its unique properties are related to its linear energy dispersion with two Dirac cones touching at a single point, and its high electron mobility. Although these properties of clean graphene have been confirmed with many different techniques, open questions remain about the interaction of foreign atoms—especially metal atoms—with graphene. A strong interaction is necessary to ensure high quality metal contacts needed for device applications, but the interaction should not be strong enough to disturb the graphene electronic structure.

The interest in the growth of magnetic metals on graphene is motivated by more specific applications in spintronics. For example, graphene sandwiched between ferromagnetic layers can serve as a spin filter [7], while materials grown on graphene are predicted to have high magnetic anisotropy [8], or to be realizations of a novel Kondo effect [9]. Graphene itself may become magnetic [10], or may serve as a platform

for high density arrays of magnetic islands for computer memory applications [11]. Electron correlations have been shown to modify the magnetic state of an adatom supported on graphene [12]. Doping with magnetic adatoms is an essential process to generate spin polarized electron current in graphene based devices.

Dysprosium (Dy), a rare earth metal, has been studied both theoretically and experimentally to determine its diffusion and adsorption energies on graphene [13]. Experimentally, scanning tunneling microscopy (STM) images were analyzed to measure the island density as a function of temperature T and coverage θ . Density functional theory (DFT) was used to calculate the potential energy surface, and the nature of the Dy–C bond. These studies have shown that the Dy–C bond is strong and that Dy can have a large potential effect on the electronic structure of graphene.

Dy grows in an hcp bulk crystal structure. Submonolayer Dy films have been studied on W(110) [14]. There, it was shown that Dy can grow as islands with hexagonal shapes and an hcp crystal structure [15, 16]. An earlier study using *in situ* resistivity and electron diffraction showed that Dy deposited on a glass substrate grows initially as an fcc crystal up to a thickness of 20 nm followed by a gradual structure change

from fcc to hcp at higher thicknesses [17]. For a different rare earth, Eu, a new fcc-like phase was found after growth on Ta(110) [18] instead of the expected bcc(110) based on the Eu bulk structure.

The step heights of fcc(111) and hcp(0001) Dy are 0.289 nm and 0.283 nm, respectively. These values are so close that the two crystal structures cannot be easily distinguished on the basis of step or island heights. Similarly, the in-plane lattice constants for fcc(111) and hcp(0001) are $a_{111} = 0.354$ nm and $a_{0001} = 0.359$ nm respectively, so it would be difficult to distinguish the two 6-fold diffraction patterns with conventional low-energy electron diffraction.

In the current study, we use STM to identify the crystal structure of Dy islands on graphene, based upon the shapes of the Dy islands. The main conclusion from the current STM study will be that Dy on epitaxial graphene grows initially as fcc(111) islands. This is evident from the triangular shaped multi-height islands which form when the islands have fully completed layers suggesting thermodynamic reasons for the fcc crystal structure. When the islands are grown under different conditions (i.e. with stepwise coverage deposition) their top layers are incomplete, but still have triangular shapes which suggests that there must also be kinetic factors responsible for the triangular shapes.

Only Dy islands show these triangular shapes among the magnetic metals studied on graphene to date: Fe, Eu, and Gd [19]. The Dy growth on graphene is also special, because it relates to shapes of multi-height islands with faceted planes at their sides, rather than only to single layer islands nucleating on top of a bulk crystal as in Pt/Pt(111) [20], Co/Cu(111) [21], and Ir/Ir(111) [22]. It would be interesting to clarify the role of graphene since bulk-like hcp(0001) islands grow on W(110) or Mo(211) [23].

2. Experiment

The method of preparing graphene on 6H-SiC(0001) depends on how fast the annealing temperature of ~ 1500 K is reached and how long the crystal is kept at this temperature [24]. By controlling these two parameters, the fraction of single to bilayer graphene can also be controlled. The determination of the graphene layer thickness relies on two methods. (1) Domain height differences which can be expressed as a combination of an integer number of single step heights of graphene, 0.33 nm, and SiC, 0.25 nm. (2) The amplitude of the $(6\sqrt{3} \times 6\sqrt{3})$ corrugation, with bilayer graphene having lower corrugation than single layer graphene for the same tunneling voltage [24]. The samples used in the current experiments have 90% single and 10% bilayer domains. The average domain size is 200 nm.

Dy is deposited using a molecular beam source with the substrate at a temperature of ~ 700 K [13] and with flux rates of 0.1–0.2 monolayers (ML) min^{-1} . The Dy source is degassed during the bakeout for several hours, so during deposition the pressure remains below 1.6×10^{-10} Torr. The number of ML of Dy is determined by finding the integrated island volume within a given area after correcting for the usual convolution tip effects. From the ratio of the integrated

volume to the product of the island area selected and the Dy fcc step height, 0.289 nm, the Dy coverage is obtained in ML.

Dy grown on graphene at room temperature and flux rates of more than 0.5 ML min^{-1} produces irregular, kinetically driven small islands. In this study Dy is grown at elevated temperatures up to 700 K to improve island crystallinity. No coarsening is observed at 700 K on the time scale of ~ 1 h, but the aspect ratio of the islands—the ratio of height to lateral size—increases. The majority of the STM images are taken at room temperature, so they reflect a frozen morphology produced at the higher deposition temperature.

3. Results

Figure 1 shows Dy deposited continuously on graphene at ~ 660 K at three different coverages: 0.29, 0.94, and 1.36 ML. The corresponding island densities are 5.5×10^{-4} islands nm^{-2} , 1.5×10^{-3} islands nm^{-2} , and 1.1×10^{-3} islands nm^{-2} . The growth mode is three-dimensional (3D) and the driving force is the low ratio ($E_a/E_c = 0.5$) of the adsorption energy ($E_a = 1.47$ eV) of Dy on graphene, to the bulk Dy bulk cohesive energy ($E_c = 2.94$ eV) as discussed in [13]. This implies that the ratio of the rates of Dy adsorption on graphene and adsorption on a bulk-like Dy island is 10^{-11} at 700 K, thus favoring 3D growth. In the experiment, we observe islands ~ 10 layers high even for small deposited amounts, as low as ~ 2 ML. This 3D growth is a general feature for all the metals grown on graphene [11, 13, 19].

For the three Dy coverages, the average island heights are 6.9 ± 1.5 layers, 7.1 ± 1.2 layers, and 8.4 ± 1.7 layers. The average areas are 84 ± 69 nm^2 , 95 ± 55 nm^2 , 159 ± 112 nm^2 respectively. In continuous deposition experiments the islands grow with fully completed layers and their sides are perfect low index planes. For hcp(0001) islands the six facet planes are equivalent with the $\{1\bar{1}01\}$ orientation. For fcc(111) islands the facet plane orientation alternates between the $\{111\}$ and $\{100\}$ orientations. The in-plane island orientation with respect to the graphene unit cell shows that the island sides are normal to the graphene (1×1) unit cell direction.

The shapes of the islands were classified into three main categories as seen in figure 1(c). Categories 1 and 2 include triangular shaped islands named TriUp and TriDown depending on the direction they are pointing, and category 3 is the Irregular Hexagon (HexIrr). Although both Gd and Dy have hcp bulk structure and Gd forms exclusively hexagonally symmetric islands on graphene after annealing to 1000 K [19], Dy shows predominantly triangular island shapes.

Categories 1 and 2 also include ‘almost triangular’ shaped islands. Examples of these ‘almost triangles’ are circled in figure 1(c). They are rhombic shapes indicating merging triangular islands and truncated islands with one or two corners missing. Diamond shaped islands were counted both in the TriUp and TriDown categories. Islands that did not fit into the three categories were labeled ‘Other’. This included the few islands that did not have six symmetric sides like the island with an arrow in figure 1(c), and islands that were too small to distinguish between hexagonal and triangular shapes like the island with an arrow in figure 1(a).

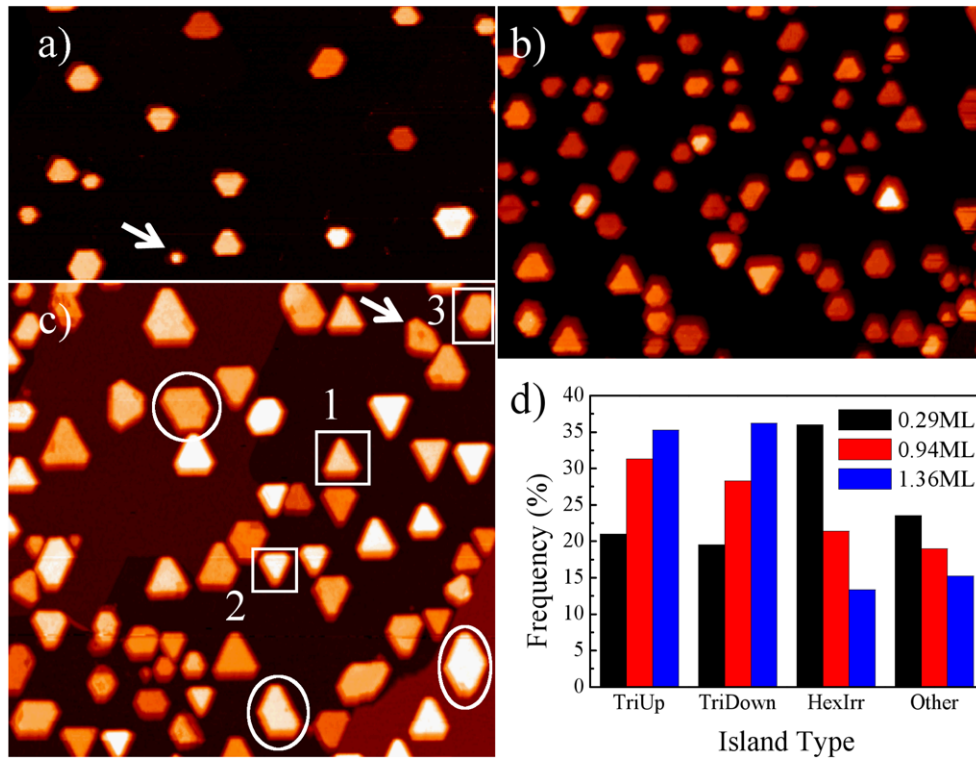


Figure 1. Dy islands grown on epitaxial graphene at 660 K after continuous deposition, with coverages of (a) 0.29 ML, (b) 0.94 ML, (c) 1.36 ML. The corresponding areas are $250 \times 150 \text{ nm}^2$, $250 \times 180 \text{ nm}^2$, and $250 \times 240 \text{ nm}^2$. The majority of the islands have triangular shapes with equal number of islands pointing in opposite directions. These are multi-height islands with perfectly completed tops. (d) Island shape histogram with the frequency of the three main categories and the shapes that are difficult to classify. As the coverage increases the fraction of triangularly shaped islands increases.

Figure 1(d) compares the relative frequency of the different types of islands. With increasing θ the relative number of triangular islands increases. This suggests that the triangular islands start as hexagonal, and as they grow they change into triangular ones.

Next we study the evolution of island shapes with θ in stepwise deposition experiments, i.e., Dy is deposited in three smaller doses, with the first coverage being 0.03 ML. This defines the initial island density, and is especially influential because of the tendency of the Dy adatoms to move to higher layers once they approach an island already nucleated. (As noted, the adsorption energy E_a for Dy on graphene is very low.) After this, 0.50 and 1.02 ML total coverages are deposited. The initial island density is 1.5×10^{-4} islands nm^{-2} , and it then increases to 3.9×10^{-4} islands nm^{-2} and 3.3×10^{-4} islands nm^{-2} . The density for 1.02 ML of figure 2(b) is 4.5 times lower than the island density of figure 1(b) at $\theta = 0.94$ ML.

Growth during continuous deposition (figure 1) is very different from growth during stepwise deposition (figure 2). Instead of growing 3D islands with the top layer complete, approximately 60% of the islands in figure 2(a) have multiple incomplete layers exposed at the top. In figure 2(a) the average size of the islands with completed tops (similar to the ones in figure 1) is $145 \pm 92 \text{ nm}^2$ while the layer islands with incomplete tops have an average size of $265 \pm 151 \text{ nm}^2$. In figure 2(b) 70% of the islands have incomplete top layers

with an average base area of $584 \pm 252 \text{ nm}^2$ while the islands with completed top layers have an average area of $352 \pm 242 \text{ nm}^2$. The larger projected area of the islands with incomplete tops versus islands with completed tops shows that they are more effective in capturing adatoms. Since the diffusing adatoms aggregate to the larger islands, this results in a smaller number of new islands nucleating and accounts for the lower island density, when compared to the continuous deposition experiments of figure 1. At the same time more atoms are necessary to cover the larger area of a given layer, which accounts for the incomplete stacked layers. The 1D line scan shown in figure 2(b) and displayed in figure 2(c) is used to measure the island height from the height increments, marked at the plateau, of the exposed edges of the incomplete top layers.

4. Discussion

As already discussed the completed multi-height triangular islands of figure 1 suggest that the grown Dy islands are fcc(111) because the side planes must be inequivalent, so three of the side planes become extinct [25]. The results of the stepwise deposition experiments with incomplete island layers shown in figure 2 suggest that growth of these islands is also kinetically limited and that the islands do not attain their equilibrium shapes under the stepwise deposition conditions. The very small, initial 0.03 ML deposition makes the island

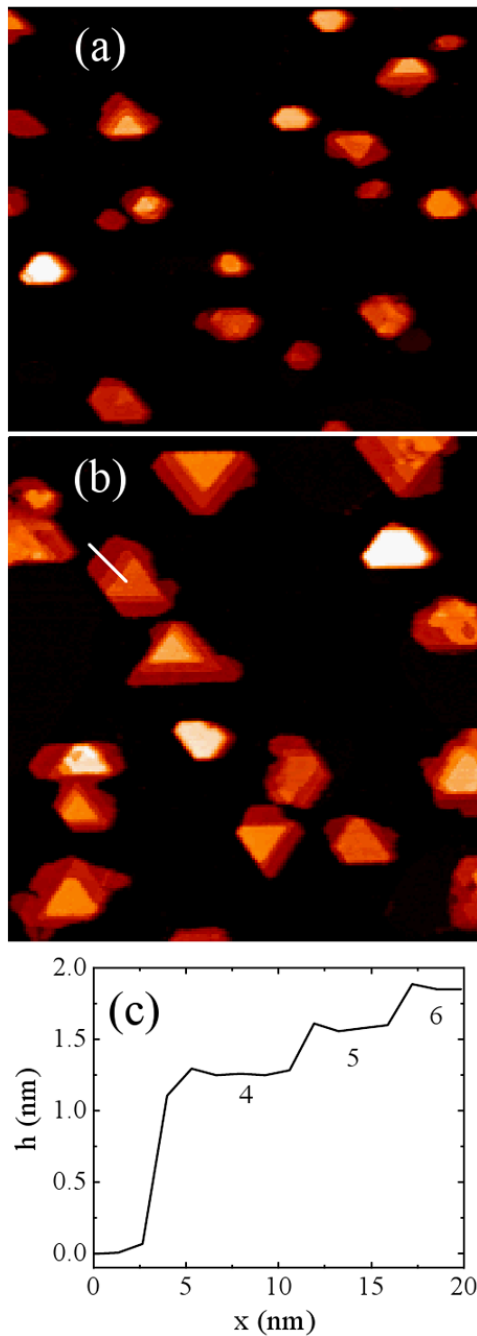


Figure 2. Dy deposition on graphene in stepwise deposition experiments following an initial 0.03 ML seeding deposition, for total coverages of (a) 0.50 ML and (b) 1.02 ML at 670 K. Images areas are (a) $185 \times 170 \text{ nm}^2$ and (b) $185 \times 200 \text{ nm}^2$. The island density is lower and the base of the islands is larger when compared to the density and base of the islands of figure 1. The initial seeding deposition determines the nucleation sites and accounts for the larger capture zone of the islands formed, which results in islands with incomplete top layers. In cases where a sequence of stacked triangular shaped islands is seen the islands point to the same direction, which shows that the islands are fcc(111). (c) 1D scan showing the heights of the exposed layers, the number showing the layer height.

density lower than that in figure 1, even at comparable coverage, because the islands formed at this early stage provide sites to which the atoms deposited at the next two

doses diffuse and aggregate [26]. Dy has relatively high mobility on graphene at 700 K.

The Dy islands form predominantly because of uphill atom flux to higher layers, caused by the lower adsorption energy E_a of metals on graphene, with a smaller contribution from atoms directly deposited on top. Since the incoming Dy atoms from the surrounding area have the tendency to move uphill, the lower incomplete layers of the islands of figure 2 do not receive enough atoms to fill the layers completely up to their edges before new layers form on top.

Figure 3 shows a schematic of the stacking of hcp(0001) layers (in (a) and (b)) and fcc(111) layers (in (c) and (d)). There are two types of edges, and their atomic arrangement is represented by the different microfacets, denoted as black rectangles (called A edges) and as black triangles (called B edges). The A edge for fcc(111) islands with fully complete layers develops into an fcc(100) plane, while the B edge develops into an fcc(111) plane. For a single layer nucleating on top of an fcc(111) island the two step types will keep their direction unchanged as more layers are built: the A edges will be in the same directions and the B edges will be at 60° . On the other hand, for hcp(0001) multi-height islands the six facet planes are equivalent $\{1\bar{1}01\}$. For single layer islands nucleating at the top of an hcp(0001) island, the same type of edges (A- and B-type) are present as for fcc(111) islands. Figure 3(a) shows that an edge in a given direction of a newly nucleated hcp(0001) island will alternate between A-type and B-type as successive layers are deposited, which implies that for triangular shaped hcp(0001) islands (because one of the inequivalent step edges is favored), the direction they are pointing would alternate with each layer.

In systems studied in the literature which show almost perfect triangular island shapes similar to ours, Monte Carlo simulations [27, 28] have shown that anisotropy in corner crossing determines the extreme triangular shapes. There are two other candidate mechanisms—anisotropy in edge sticking and anisotropy in edge diffusion—but when these and corner crossing are both present corner crossing is often the dominant process that controls the island shape. More specifically, in simulations using barriers relevant to the Al/Al(111) system calculated with density functional theory it was found that the barriers for atoms to cross the island corner clockwise versus counterclockwise differ by 0.17 eV at 160 K, and perfect triangular shapes result. For the Co/Cu(111) system, the combined effect of differences in edge diffusion and a corner crossing barrier of 0.31 eV at 300 K [28] also results in perfect triangular shapes. The two simulations have an anisotropic corner crossing ratio of $\sim 10^5$ for the atoms moving from one island edge around the corner to the adjacent edge. It was argued that the net effect is for the corner to serve as a reflecting wall for the approaching atoms from the direction with the higher barrier, thus making the atom population on the incoming step higher, resulting in this step growing faster and at the end being eliminated. Similar barriers as those found in [28] can be applicable to the growth of the Dy triangular nano-islands, since despite the higher growth temperature of 700 K, using the barriers of [27, 28] the ratio between the two rates to cross a corner in the two opposite directions will still be high, 1.4×10^2 .

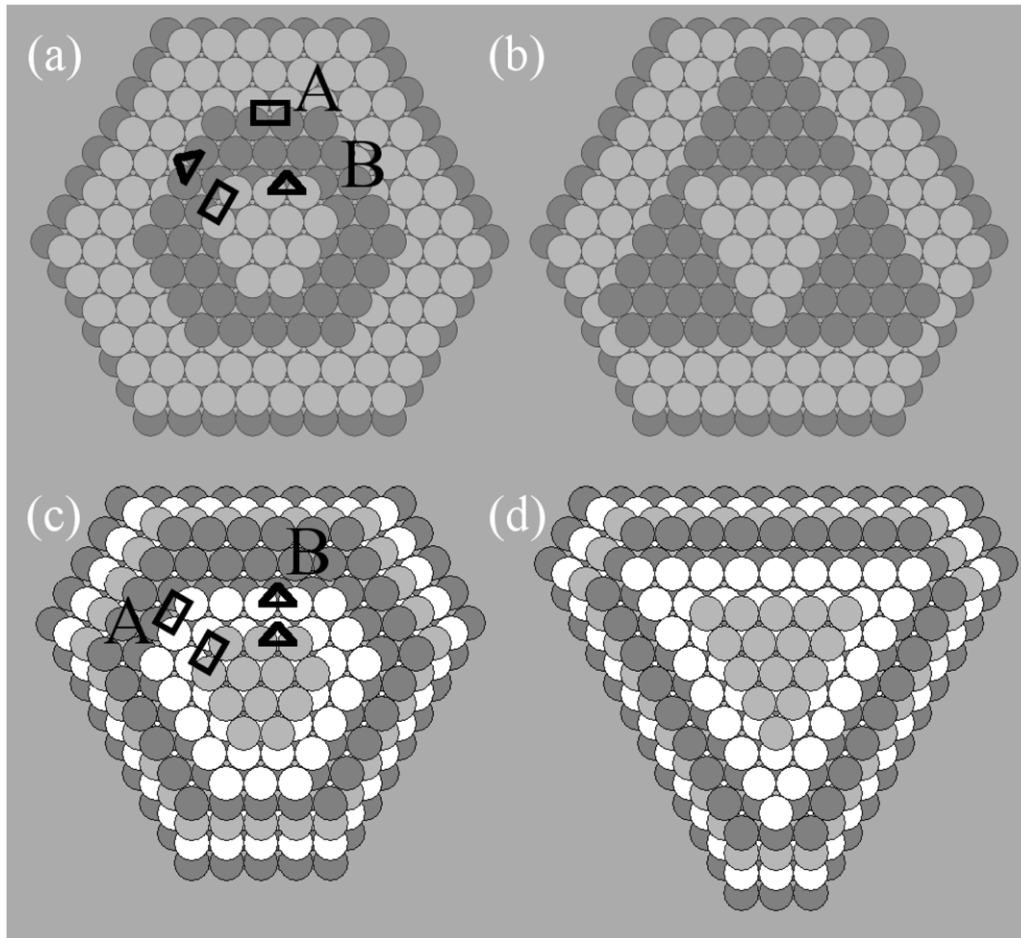


Figure 3. Models of incomplete island nucleation on the top layers. The edges of the single layer islands have two types of steps—A and B—distinguished by the different microfacets: black rectangles for A steps and black triangles for B steps. (a) and (b) show the case of hcp(0001) crystal growth with the triangular island direction in successive layers alternating. Fcc(111) triangular islands shown in (c) and (d) point in the same direction at all layers.

As seen in figures 1 and 2 the number of islands pointing in opposite directions are essentially the same and the islands keep this preferred direction as their height increases. This is expected for fcc(111) islands since there are two possible stackings: ABCABC and ACBACB. Both stackings should have the same probability. Dy on graphene is a heteroepitaxial system and both types of stackings nucleate initially with equal probability, because the graphene substrate structure is not correlated to the growing metal island structure.

In contrast, the homoepitaxial growth of Mg on Mg(0001) films grown on W(110) seen in figure 4 also results in perfect single layer triangular Mg islands nucleating instead of hexagonal islands as expected from the Mg bulk hcp structure. However, the newly nucleated Mg(0001) islands alternate in the direction they point to with each new layer, in agreement with the schematics of figures 3(a) and (b) [23]. Their shape is also a result of extreme corner crossing anisotropy. For hcp(0001) islands, only one stacking is possible and each terrace should have triangular shaped islands pointing 100% in either up or down direction. Terraces differing by one layer should also have 100% of the islands reversed by 180° from the orientation in the previous layer. This is exactly what is observed for homoepitaxial Mg/Mg(0001) growth in figure 4.

5. Conclusions

It has been reported in the literature that several epitaxially grown metal/metal systems exhibit islands that do not have the hexagonal shapes expected from the six-fold symmetry of the bulk metal, but instead they have either asymmetric hexagonal shapes or, in a few cases, perfect triangular shapes. The majority of these experiments involve single or bilayer islands nucleating on top of a macroscopic single crystal surface or on top of very large islands [29]. The Dy/graphene system distinguishes itself from both of these categories with multi-height triangularly shaped islands that have the fcc(111) rather than hcp(0001) crystal structure. Single layer triangular islands observed on incomplete layers on Dy islands grown in stepwise deposition experiments suggest that in addition to the thermodynamic reasons, kinetic ones must also be responsible for the island triangular shapes. The kinetic reasons most likely are related to a corner crossing barrier anisotropy. It would be interesting to investigate experimentally and theoretically the magnetic moment and magnetic domain distribution in these fcc(111) Dy islands to compare them to the corresponding properties of normal hcp(0001) Dy islands.



Figure 4. Mg(0001) 15 ML film (grown on W(110)) after deposition of additional 0.1 ML of Mg at 135 K with 0.017 ML s^{-1} flux rate. Image size is $250 \times 170 \text{ nm}^2$. The triangularly shaped single layer Mg islands, caused by extreme corner crossing anisotropy, alternate in direction with increasing layer height, but within each terrace they point along the same direction with essentially $\sim 100\%$ frequency, as expected for hcp(0001) islands.

Acknowledgment

This work was supported by the Office of Science, Basic Energy Sciences, Materials Sciences and Engineering Division of the US Department of Energy (USDOE), under Contract No. DE-AC02-07CH11358 with the US Department of Energy.

References

- [1] Berger C *et al* 2004 *J. Phys. Chem. B* **108** 19912
- [2] Novoselov K S *et al* 2004 *Science* **306** 666
- [3] Castro Neto A H *et al* 2009 *Rev. Mod. Phys.* **81** 109
- [4] Miller D L *et al* 2010 *Nature Phys.* **6** 811
- [5] Winterlin J and Bocquet M-L 2009 *Surf. Sci.* **603** 1841–52
- [6] Hattab H *et al* 2012 *Nano Lett.* **12** 678
- [7] Karpan V M *et al* 2007 *Phys. Rev. Lett.* **99** 176602
- [8] Vo-Van C *et al* 2010 *New J. Phys.* **12** 103040
- [9] Uchoa B, Rappoport T G and Castro Neto A H 2011 *Phys. Rev. Lett.* **106** 016801
- [10] Sevinçli H, Topsakal M, Durgun E and Ciraci S 2008 *Phys. Rev. B* **77** 195434
- [11] Binz S, Hupalo M, Liu X, Wang C Z, Lu W-C, Thiel P A, Ho K M, Conrad E H and Tringides M C 2012 *Phys. Rev. Lett.* **109** 026103
- [12] Rudenko A N *et al* 2012 *Phys. Rev. B* **86** 075422
- [13] Hupalo M, Liu X, Wang C Z, Lu W C, Yao Y X, Ho K M and Tringides M C 2011 *Adv. Mater.* **23** 2082
- [14] Kolaczkiwicz J and Bauer E 1986 *Surf. Sci.* **175** 487
- [15] Li H, Tian D, Quinn J, Li Y S, Wu S C and Jona F 1992 *Phys. Rev. B* **45** 3853
- [16] Krause S, Berbil-Bautista L, Hänke T, Vonau F, Bode M and Wiesendanger R 2006 *Europhys. Lett.* **76** 637
- [17] Kaul V K, Bist B M S and Srivastava O N 1975 *Thin Solid Films* **30** 65–72
- [18] Olson C G, Wu X, Chen Z L and Lynch D W 1995 *Phys. Rev. Lett.* **74** 992
- [19] Hupalo M, Binz S and Tringides M C 2011 *J. Phys.: Condens. Matter* **23** 045005
- [20] Michely T, Hohage M, Bott M and Comsa G 1993 *Phys. Rev. Lett.* **70** 3943–6
- [21] Prieto J E, de la Figuera J and Miranda R 2000 *Phys. Rev. B* **62** 2126
- [22] Busse C, Polop C, Müller M, Albe K, Linke U and Michely T 2003 *Phys. Rev. Lett.* **91** 056103
- [23] Hupalo M *et al* 2013 unpublished
- [24] Hupalo M, Conrad E H and Tringides M C 2009 *Phys. Rev. B* **80** 041401
- [25] Bonzel H P, Yu D K and Scheffler M 2007 *Appl. Phys. A* **87** 391
- [26] Rosenfeld G, Servaty R, Teichert C, Poelsema B and Comsa G 1993 *Phys. Rev. Lett.* **71** 895
- [27] Ovesson S, Bogicevic A and Lundqvist B I 1999 *Phys. Rev. Lett.* **83** 2608
- [28] Negulyaev N N, Stepanyuk V S, Bruno P, Diekhöner L, Wahl P and Kern K 2008 *Phys. Rev. B* **77** 125437
- [29] Evans J W *et al* 2006 *Surf. Sci. Rep.* **61** 1